*Research Article*

# Rotor Temperature Safety Prediction Method of PMSM for Electric Vehicle on Real-Time Energy Equivalence

**Anjian Zhou [ID],[1,2] Changhong Du,[2] Zhiyuan Peng,[2] Qianlei Peng,[2] and Datong Qin[1]**

[1]*State Key Laboratory of Mechanical Transmission & School of Automotive Engineering, Chongqing University, Chongqing 400044, China*
[2]*Chongqing Changan New Energy Automobile Technology Co., Ltd., Chongqing 401133, China*

Correspondence should be addressed to Anjian Zhou; 20183201027g@cqu.edu.cn

The load capacity of the permanent magnet synchronous motor is limited by the rotor temperature, and the excessive temperature of the rotor will bring potential thermal safety problems of the system. Therefore, the accurate prediction of the rotor temperature of the permanent magnet synchronous motor for the electric vehicle is crucial to improve the motor performance and system operation safety. This paper studied the heating mechanism and the energy flow path of the motor and built the heat energy conversion model of the stator and rotor. The real-time algorithm to predict the rotor temperature was constructed based on the dissipative energy conservation of the stator of the motor rotor temperature. And the prediction method of the initial rotor temperature is fitted using the experimental results when the system is powered on. Finally, the test platform was set up to validate the rotor temperature accuracy. The results show that the motor rotor temperature estimation error under the dynamic operating condition is within ±5. The research provides a solution to improve the performance and thermal safety of the permanent magnet synchronous motor for electric vehicles.

## 1. Introduction

The permanent magnet synchronous motor (PMSM) is widely used in pure electric vehicles due to high-power density, high efficiency, and high torque. Thermal safety and peak performance are the difficulties of PMSM development. The copper and the iron losses are the main sources for the temperature rise of rotor magnetic steel, and the temperature of rotor magnetic steel directly determines the duration of the peak power of the motor. Therefore, the research of the rotor temperature prediction can not only ensure the thermal safety of the motor but also improve the peak performance of the motor. Meanwhile, the coercive force of magnetic steel is closely related to temperature, which decreases with the rise of temperature. When the temperature of the rotor magnetic steel exceeds the limit value, the irreversible demagnetization will happen. In general, the irreversible demagnetization should be avoided under the operating condition of the motor [1–3]. In fact, the torque

capacity of PMSM is usually lower than its actual torque capacity to avoid overheating failure of the motor without the high-precision rotor temperature prediction [4, 5].

It is difficult to obtain the temperature of rotor magnetic steel by direct measurement when the motor is running [6]. The rotor temperature measurement methods include sliding ring and wireless temperature sensor. But these two methods have high cost and low engineering feasibility, so they cannot be applied in batch. Compared with the direct temperature measurement with an integrated sensor to the rotor, a mature rotor temperature algorithm has advantages in development cost and fast response of thermal protection [7, 8]. But the real-time rotor temperature prediction technology faces some challenges, such as thermal model complexity, algorithm safety, and temperature prediction accuracy [9]. In the current research, the rotor temperature prediction methods mainly include three directions. The first method predicts the rotor temperature with the empirical formula by the indirect variables [10]. The second method is to subdivide the motor

into elements, establish the thermal resistance between elements, and form the thermal network model [11]. The third method is to measure the counterelectromotive force of the motor and calculate the residual flux density of the motor [12]. The actual rotor temperature is obtained by querying the corresponding relationship between the residual flux density and the rotor temperature [13, 14].

Nevertheless, there are some shortcomings in these research methods. Firstly, the temperature change of the rotor of the motor under natural cooling condition is not taken into account after the whole vehicle system is powered down. As a result, the initial temperature of the rotor cannot be assigned to calculate when the system is powered up again. Secondly, it only predicts the rotor temperature under normal temperature conditions without considering the influence of ambient temperature on the rotor temperature characteristics, resulting in poor adaptability and limited accuracy of the algorithm [15]. In addition, when measuring the rotor temperature with the counterelectromotive force method, the motor current should be unloaded. It is not practical to predict the real working condition of the vehicle. This paper will comprehensively consider the thermal nodes that affect the rotor temperature of the motor, and obtain the law of the rotor temperature characteristics of the motor through the test method. The rotor temperature algorithm is built under different environmental temperatures and load conditions, so as to improve the performance and operation safety of the motor system [16, 17].

## 2. Main Problem

To predict the temperature of the rotor accurately, the mechanism of heat generation and conduction for the motor should be researched. Considering the complexity of the thermal characteristics on the actual motor work condition, the energy transfer paths inside the motor system were simplified as shown in Figure 1.

The temperature rise of the rotor is affected by the copper loss $P_{cu}$, the iron loss $P_{iron}$, the mechanical loss $P_{mech}$, and the coolant dissipation $P_w$ [18–20]. The loss exchanges with the environment in the form of heat to attain the thermodynamic equilibrium. Meanwhile, the stator generates loss or heat when the three-phase current reacts on the stator. As a source, the stator would heat on the rotor with a power of $P_r$, dissipate to the air with a power of $P_{s-air}$, and dissipate to the coolant with a power of $P_w$. Also, the rotor would dissipate to the air with a power of $P_{r-air}$.

As a main heat source of the stator, the copper loss is caused by three-phase current passing through the stator winding cross section. To eliminate the irregularity of stator current in the winding, the current in the stator winding section is simplified and equivalent to uniform distribution. The copper loss is estimated by the following formula [21, 22]:

$$P_{Cu} = nI_{phase}^2 R_{phase},$$
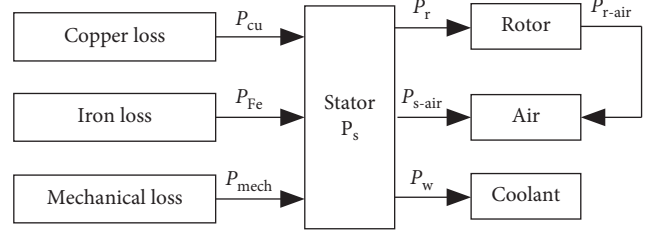$$R_{phase} = R_{20}\frac{(235 + T_{en})}{(235 + 20)}, \tag{1}$$



Figure 1: The energy transfer paths of the motor system.

where $n$ is the phase number of the motor, $I_{phase}$ is the phase current, $R_{phase}$ is the phase resistance, $R_{20}$ is the resistance of the stator winding at an ambient temperature of 20, and $T_{en}$ is the ambient temperature.

The iron loss includes the hysteresis loss and the eddy current loss. The hysteresis loss is caused by the change of alternating magnetic field caused by the alternating current in the stator winding. The eddy current loss is caused by the induced current as the magnetic field changes in the core. The iron loss is calculated by the following formula [23, 24]:

$$P_{iron} = k_h f B_m^2 + k_e f^2 B_m^2, \tag{2}$$

where $k_h$ is the hysteresis loss coefficient, $k_e$ is the eddy current loss coefficient, $f$ is the armature field alternating frequency, and $B_m$ is the amplitude of flux density of the stator core.

The mechanical loss consists of the bearing friction loss and the windage loss. The mechanical loss is calculated by the following formula [25, 26]:

$$P_{mech} = k_c C_f \pi \rho_{air} \omega_m^3 r^4 l, \tag{3}$$

where $k_c$ is the coefficient of surface roughness, $C_f$ is the friction coefficient, $\pi$ is the constant parameter of Pi, $\rho_{air}$ is the density of air, $\omega_m$ is the angular velocity of the rotor, $l$ is the length of the rotor, and $r$ is the radius of the rotor.

As the motor works, most of the heat is taken away by the coolant and the rest is carried away by air. The heat dissipated by the coolant is estimated by the following formula [27, 28]:

$$P_w = \rho_w C_w A_w v \frac{(T_{in} - T_{out})}{(t_2 - t_1)}, \tag{4}$$

where $\rho_w$ is the density of the coolant, $C_w$ is the specific heat of the coolant, $A_w$ is the section area of the cooling pipe, $v$ is the flow velocity of the coolant, $T_{in}$ and $T_{out}$ are the temperatures of the coolant at the inlet and the outlet, and $t_1$ and $t_2$ are the beginning and the ending time.

The heat carried away by air is evaluated by the following formula [29].

Its Newton function is given by

$$P_{s-air} = \delta A_s \frac{(T_s - T_{en})}{(t_2 - t_1)},$$
$$P_{r-air} = \alpha A_r \frac{(T_r - T_{en})}{(t_2 - t_1)}, \tag{5}$$

where $\delta$ and $\alpha$ are the coefficients of convection heat transfer for the stator and the rotor [30], $A_s$ is the area of convection heat transfer between the stator surface and the air, $A_r$ is the area of convection heat transfer between the rotor surface and the air, and $T_s$ and $T_r$ are the temperatures at the surface of the stator and the rotor:

$$\begin{cases} \delta = 9.73 + 14V_s^{0.62}, \\ \alpha = 9.73 + 14V_r^{0.62}, \end{cases} \tag{6}$$

where $V_s$ and $V_r$ are the air velocity of the cooling surface for the stator and the rotor, respectively.

The estimation accuracy of rotor temperature is greatly influenced by factors of motor operation condition and environment temperature. In order to obtain high accuracy rotor temperature, equivalent and accurate modeling solutions will be used to build a rotor temperature model based on the running state and stop state, respectively.

It is clear that the heating power of the stator mainly consists of three parts including copper loss, iron loss, and mechanical loss according to the energy flow analysis during motor running state from Figure 1. The conservation of energy can be expressed as follows.

From this, the decision function corresponding to the segmentation hyperplane equation can be solved, which is given by

$$P_s = P_{Cu} + P_{iron} + P_{mech}. \tag{7}$$

The absorbing energy of the stator will change its temperature during the period of time, so it is concluded as follows:

$$P_s = C_s M_s \frac{(T_{s2} - T_{s1})}{(t_2 - t_1)}, \tag{8}$$

where $C_s$ is the specific heat of the stator, $M_s$ is the mass of the stator, $T_{s1}$ and $T_{s2}$ are the stator temperatures at interval time points of sample period, respectively, and $t_1$ and $t_2$ are interval time points of sample periods, respectively.

Meanwhile, the stator will bring heat energy to cooling water, atmosphere, and rotor as a heating energy resource. Therefore, the absorbing heat power of the rotor can be concluded based on the conservation of energy as follows:

$$P_s = P_r + P_w + P_{s-air} + P_{r-air}. \tag{9}$$

The absorbing energy of the rotor will change its temperature during the period of time, so it is concluded as follows:

$$P_r = C_r M_r \frac{(T_{r2} - T_{r1})}{(t_2 - t_1)}, \tag{10}$$

where $C_r$ is the specific heat of the rotor, $M_r$ is the mass of the rotor, and $T_{r1}$ and $T_{r2}$ are the rotor temperatures at interval time points of the sample period, respectively.

## 3. Method

Due to the rotor temperature variation during motor running state, updating of the rotor temperature can be attained by putting the previous rotor temperature into formula (10) and adopting a real-time iterative algorithm per operation period. Therefore, combine formulas (8) and (9) to build an estimation model of rotor temperature as follows:

$$T_{r-act} = T_{r2} = T_{r1} + \Delta T_r,$$

$$\Delta T_r = \frac{C_s M_s (T_{s2} - T_{s1}) - (P_w + P_{s-air} + P_{r-air})(t_2 - t_1)}{C_r M_r}, \tag{11}$$

where $T_{r-act}$ is the real-time rotor temperature from the estimation model.

When the motor comes into a stop state, the heat energy of the rotor brings to the atmosphere and its temperature goes down to the environment temperature along stop time. Therefore, the rotor temperature model under the motor stop state can be attained by obtaining the relationship between rotor temperature and stop time.

When the vehicle is powered on, initial rotor temperature can be attained by adopting the previous rotor temperature $T_{r-pre}$, the stop time $t_{stop}$, and the environment temperature $T_{en}$ as the following steps:

(1) Obtain the value of $T_{r-pre}$ and $t_{stop}$ which are saved in electrically erasable programmable read-only memory (EEPROM) of the motor controller last time.

(2) Receive the environment temperature $T_{en}$ from the air-conditioning controller, and initialization time point $t_0$ can be captured by looking up the table of rotor temperature and the stop time from Figure 2 at different environment temperatures $T_1$ and $T_2$.

(3) According to $t_{stop}$ and $t_0$ from step (1) and step (2), initial rotor temperature $T_{r-init(T1)}$ and $T_{r-init(T2)}$ of different environment temperatures $T_1$ and $T_2$ can be obtained by looking up the table of rotor temperature and stop time from Figure 2 at the time point of $t_0 + t_{stop}$.

(4) Based on output results from step (3), rotor initial temperature at different environment temperatures $T_{en}$ can be matched as follows:

$$T_{r-init(T)} = \xi T_{r-init(T1)} + (1 - \xi)T_{r-init(T2)}, \tag{12}$$

where $\xi$ is the matching coefficient depending on environment temperature as shown in Table 1.

A real-time control algorithm is constructed to estimate the rotor temperature at different environment temperatures and operation states based on the rotor temperature model. The algorithm process and software frame are introduced in Figure 3.

Firstly, it is necessary to make sure whether the system is powered on or not, and then judge motor operation state by actual motor torque and speed. When the motor comes into stop state (Flg = 0), initial rotor temperature is attained by the estimation model in the stop state. Next step, when motor torque and speed are checked by controller, real-time
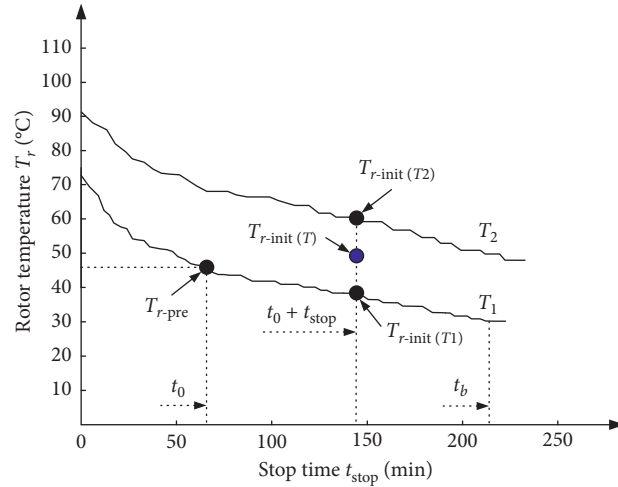
Figure 2: The relationship between rotor temperature and stop time.

Table 1: The matching coefficient for the rotor initial temperature.

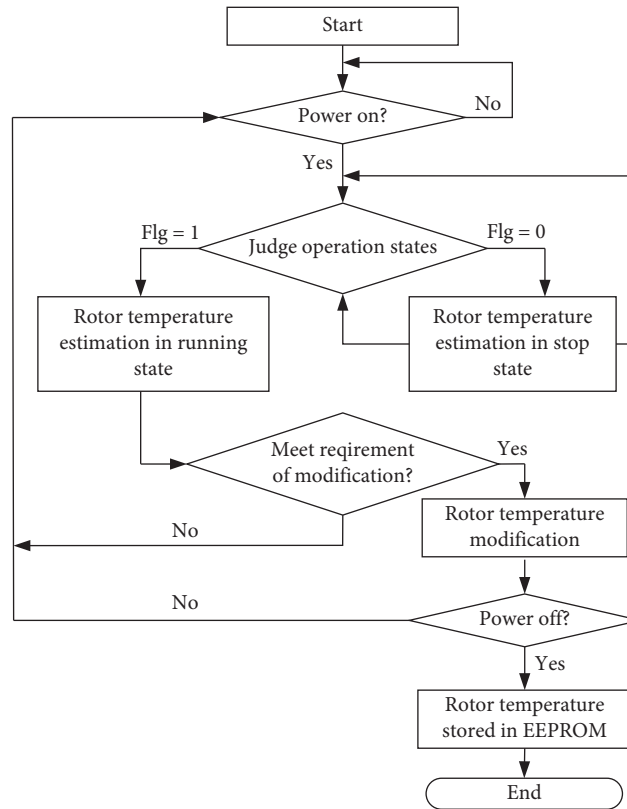| $T_{en}$ | 0°C–10°C | 10°C–20°C | 20°C–30°C | 30°C–40°C | 40°C–50°C | 50°C–60°C | 60°C–70°C |
|---|---|---|---|---|---|---|---|
| $\xi$ | 0.1 | 0.3 | 0.3 | 0.5 | 0.5 | 0.1 | 0.1 |



Figure 3: The algorithm process of rotor temperature.

rotor temperature is calculated by the estimation model in running state. Rotor temperature needs to be modified during the motor running state if it meets the requirement of the modification strategy. Finally, when it comes into power off for the system, real-time rotor temperature is stored into the memorizer of EEPROM and the previous rotor temperature can be used again in next power on for the system.

There is an accumulative error to adopt a real-time iterative algorithm to estimate rotor temperature. Therefore, it

is necessary to build a modification strategy to improve the estimation accuracy of rotor temperature as follows:

$$n_{\text{cal}-1} \le |n_{\text{mot}}| \le n_{\text{cal}-2},$$
$$|T_{\text{mot}-\text{trq}}| \le T_{\text{cal}},$$
$$\Delta\psi_{\text{mot}} \le \Delta\psi_{\text{cal}}, \tag{13}$$

where $n_{\text{mot}}$ is the actual motor speed, $n_{\text{cal}-1}$ and $n_{\text{cal}-2}$ are low- and high-level limitation of motor speed, respectively, $T_{\text{mot}-\text{trq}}$ is the actual motor torque, $T_{\text{cal}}$ is the motor torque limitation, $\Delta\psi_{\text{mot}}$ is the changing rate of motor actual flux linkage, and $\Delta\psi_{\text{cal}}$ is the changing rate limitation of motor flux linkage.

It is necessary to limit the changing rate to eliminate the prominent variation between estimation value and modification value and avoid power break-off or torque cut-down in a short time. Therefore, the updated value of rotor temperature in a running period should be modified based on the following equation:

$$T_{\text{var}} = T_{r-\text{act}} + k\left(T_{\text{tab}} - T_{r-\text{act}}\right), \tag{14}$$

where $T_{\text{tab}}$ is the rotor temperature from looking up the flux linkage table for motor and $k$ is the changing rate for rotor temperature modification.

The numerical model of the rotor temperature algorithm is built by relevant experiments and embedded in the software of the motor control system to satisfy the practicability of the rotor temperature algorithm.

According to the algorithm established above, the prediction of the rotor temperature will produce accumulated errors with the extension of calculation time. In order to ensure the accuracy of rotor temperature prediction, equation (14) is used to correct the rotor temperature.

Firstly, the counterelectromotive force of the motor corresponding to each rotor temperature was obtained through experiments. And the motor flux was calculated by using the following formula:

$$\psi_{\text{mot}} = \frac{E_\varphi}{\omega_{\text{mot}}} = \frac{7.8 E_{\text{mot}}}{\eta_{\text{mot}} p_{\text{mot}}}, \tag{15}$$

where $E_\varphi$ is the maximum phase electromotive force, $\omega_{\text{mot}}$ is the electrical angular frequency, $E_{\text{mot}}$ is the phase electromotive force, and $p_{\text{mot}}$ is the pole pairs of the motor.

As a result, the numerical model of the motor flux and rotor temperature was built, as shown in Figure 4.

The total cooling dissipation of the motor includes three parts: cooling water dissipated power and stator and rotor dissipated power to air. The relationship between the total cooling dissipation of the system and the stator temperature change rate is established as shown in Figure 5. The calibration and optimization of the numerical model were carried out by experiments under different load conditions to improve the prediction accuracy of the rotor temperature model.

In order to obtain the initial rotor temperature when the motor system is powered on, the numerical model is established corresponding to the rotor temperature and downtime under the state of natural cooling of the motor system. The
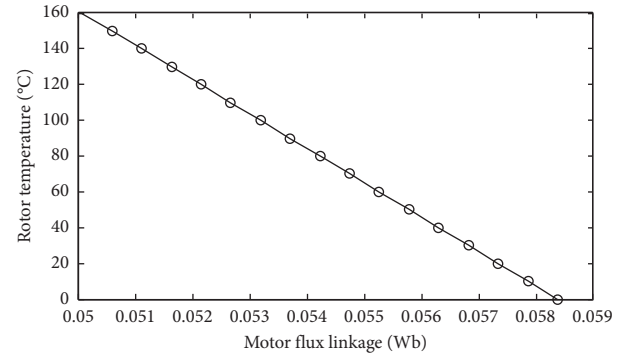


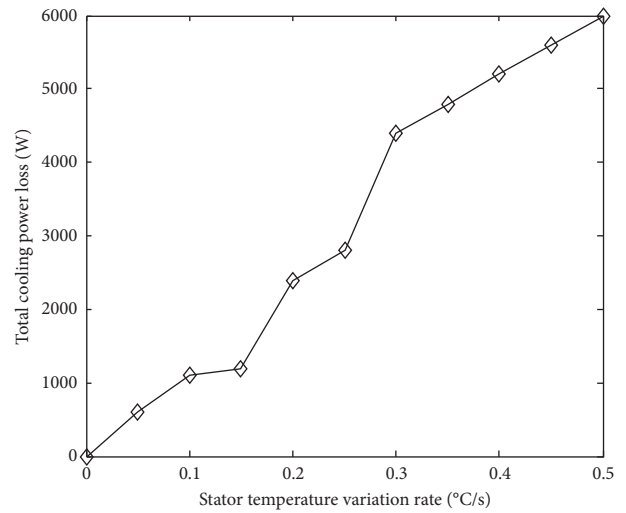Figure 4: The relationship between the rotor temperature and the motor flux linkage.



Figure 5: The numerical model of the total cooling dissipation.

motor was run at high power until the rotor temperature rose to the equilibrium point at each ambient temperature under the conditions of 10°C, 30°C, 50°C, and 70°C, respectively. And the expression of rotor temperature and shutdown time was fitted by the polynomial, as shown in Figures 6–9.

## 4. Results

To validate the real-time control algorithm of the rotor temperature prediction model established in this paper, an AVL test system is used to build a motor rotor temperature accuracy experimental platform, as shown in Figure 10. A slip ring is used to draw out the thermal resistance for the rotor temperature, as shown in Figure 11. The experimental platform consists of power dynamometer, battery simulator, temperature box, cooling system, motor system, electrical parameter tester, adjustable low-voltage power supply, and related sensors.

To ensure the prediction accuracy of the algorithm in the different environment temperatures under the condition of changing load, the motor was running under different loads in the ambient temperature 30°C and 70°C, respectively. As shown in Figures 12–14, the maximum error between the prediction value and the experimental results under fixed load conditions is within ±6°C.
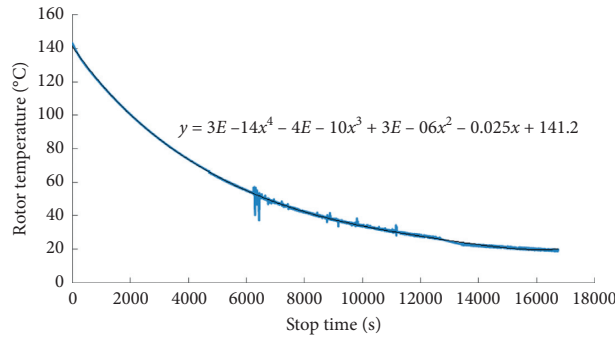
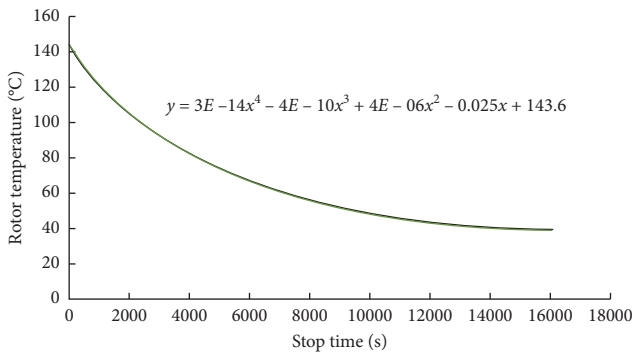FIGURE 6: The rotor temperature curve at environment temperature 10°C.



FIGURE 7: The rotor temperature curve at environment temperature 30°C.
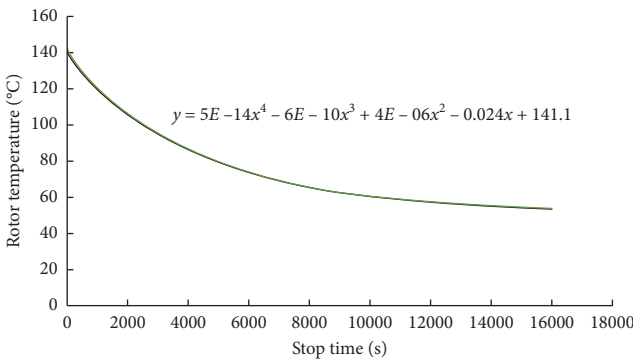


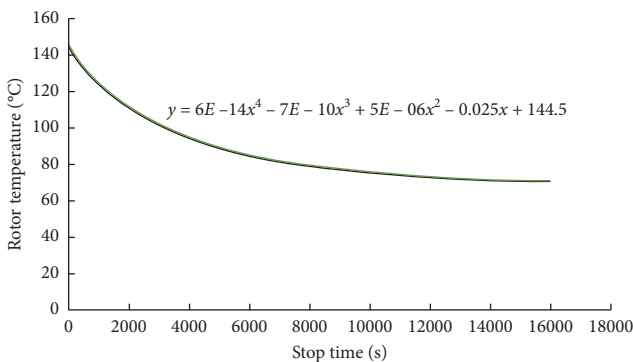FIGURE 8: The rotor temperature curve at environment temperature 50°C.



FIGURE 9: The rotor temperature curve at environment temperature 70°C.
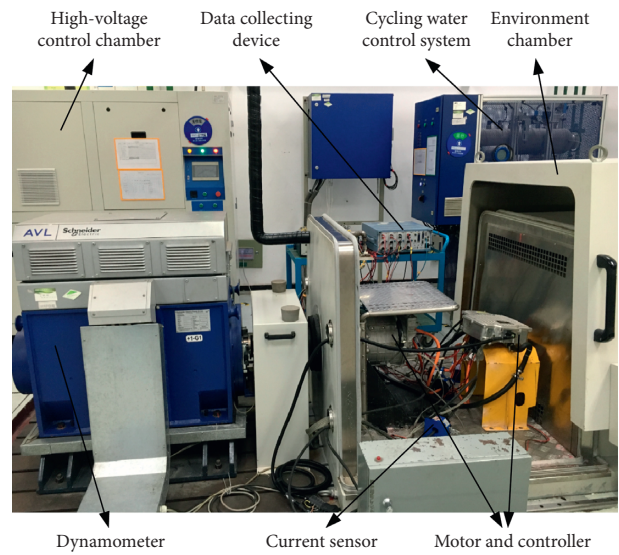


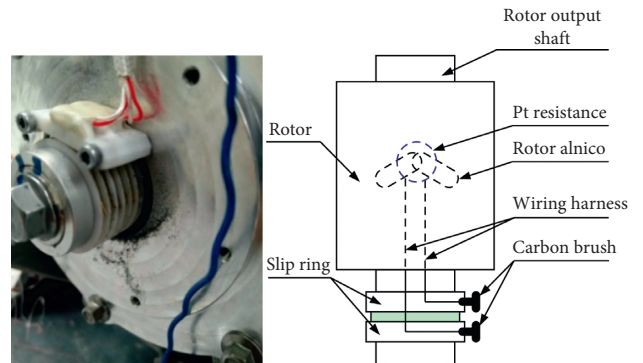FIGURE 10: The motor rotor temperature accuracy experimental platform.



FIGURE 11: The schematic of the rotor temperature test using the slip ring.

To validate the proposed algorithm accuracy rotor temperature under the changing load condition, the motor was running with the vehicle real variable load in the environment temperatures of 30°C and 70°C, respectively. The comparison indicates that the maximum dynamic error is within ±5°C between the predicted and the measured values, as shown in Figures 15 and 16.
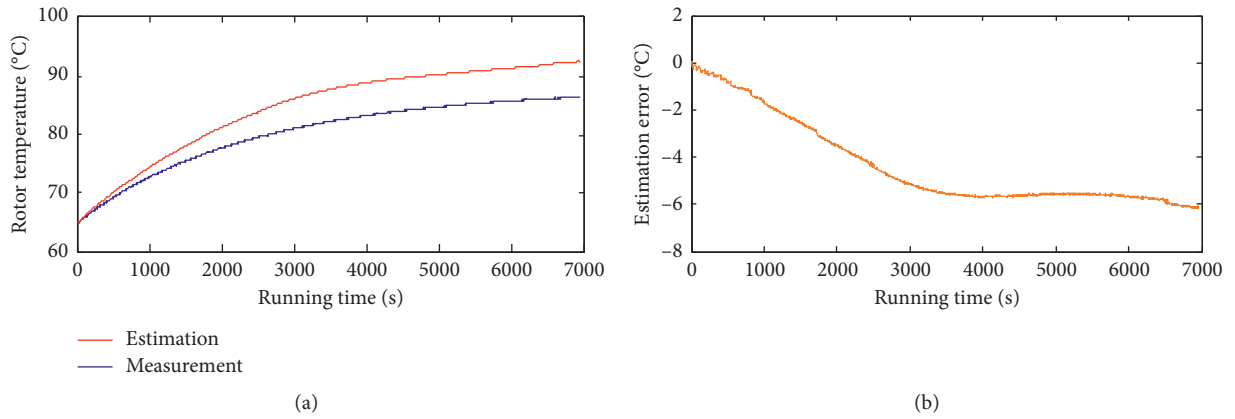
(a)

(b)

FIGURE 12: The relationship between the rotor temperature and the motor flux linkage.
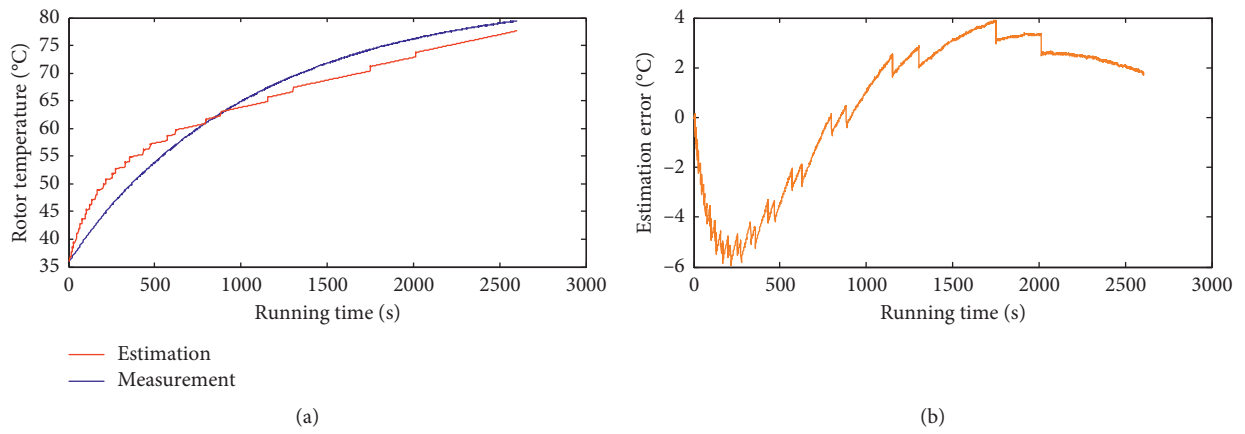


(a)

(b)

FIGURE 13: Test results at constant load condition (5000 rpm/68 Nm and environment temperature 30°C).
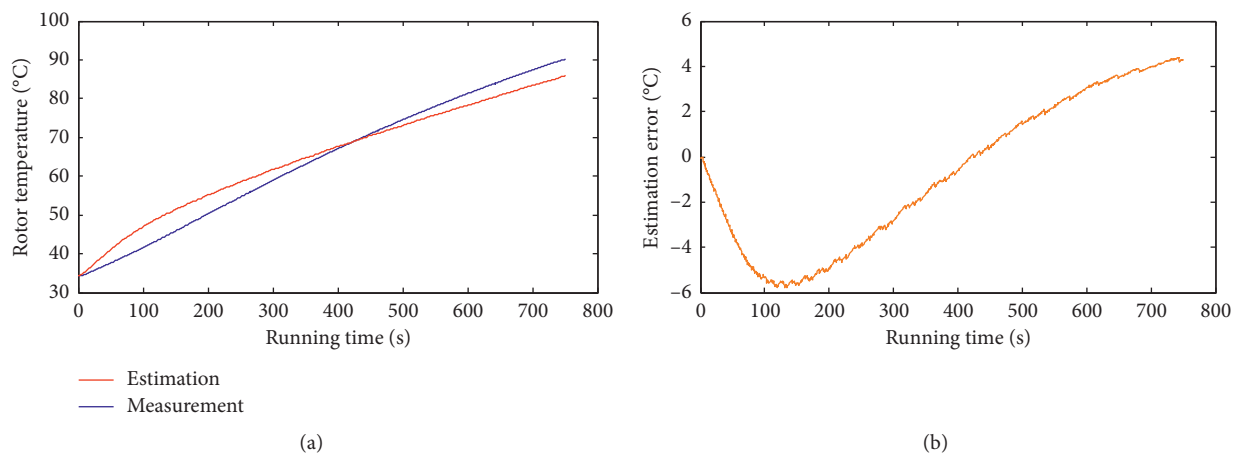


(a)

(b)

FIGURE 14: Test results at constant load condition (4000 rpm/193 Nm and environment temperature 30°C).
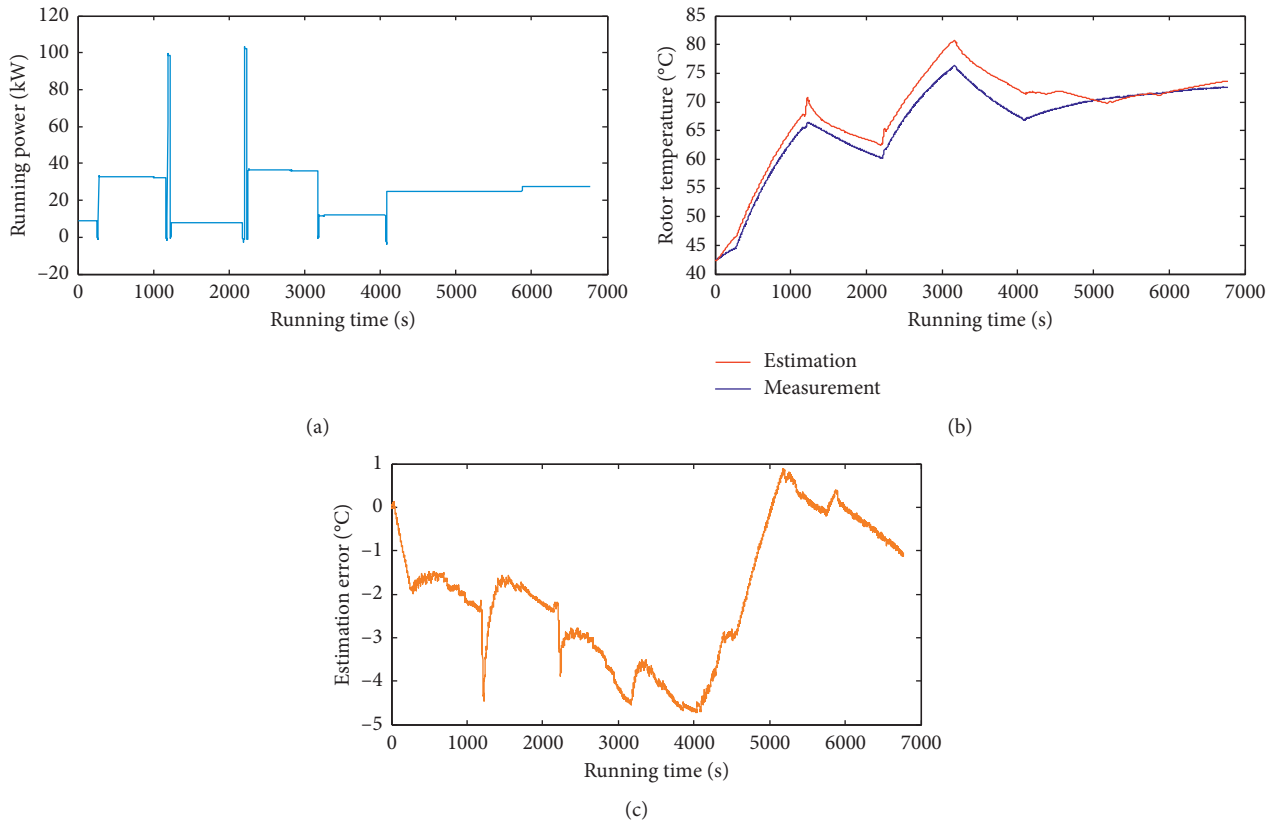
(a)

(b)

(c)

FIGURE 15: Test results at variational load condition (environment temperature 30°C).
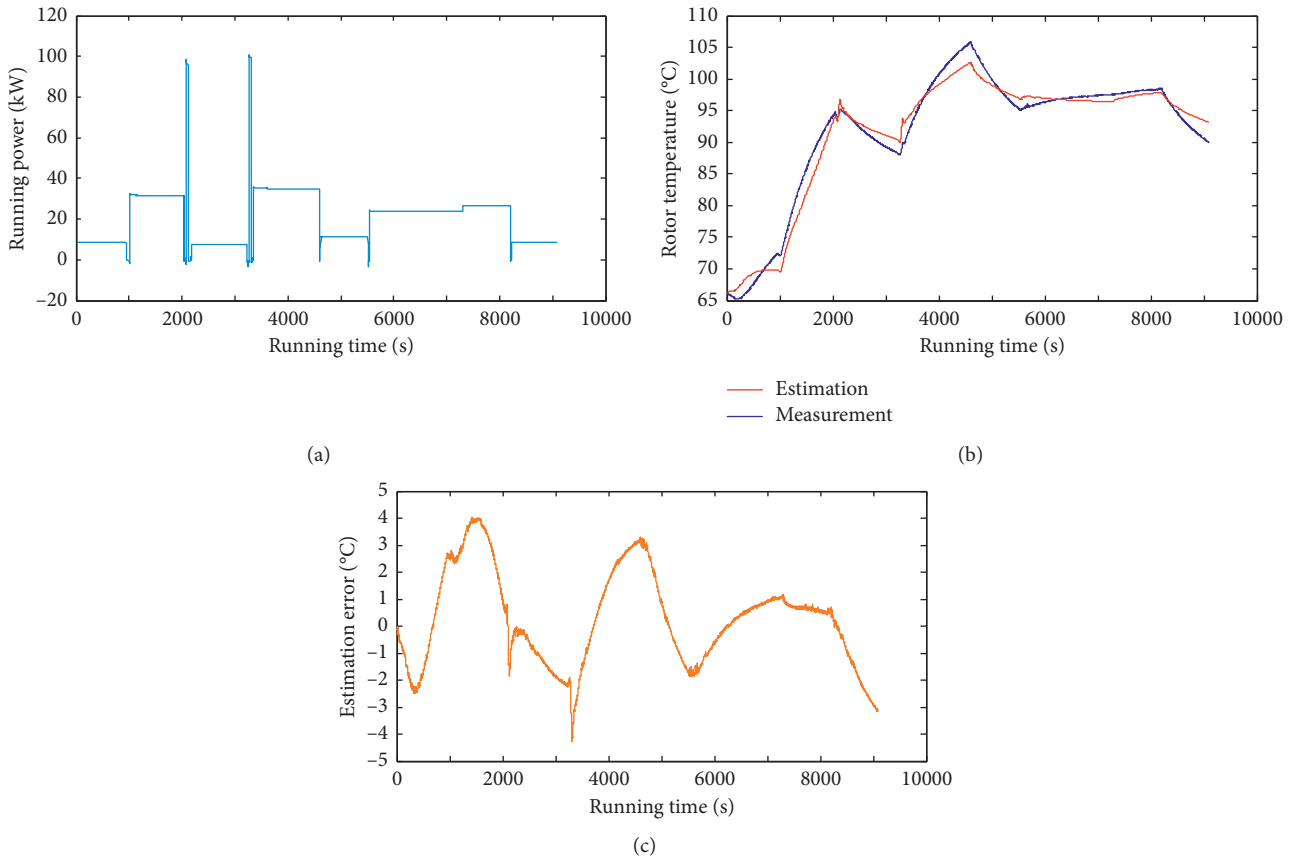


(a)

(b)

(c)

FIGURE 16: Test results at variational load condition (environment temperature 70°C).

## 5. Conclusion

A method to estimate the rotor temperature of the permanent magnet synchronous motor in this paper has been proposed. The method is characterized with the equivalent thermal model of rotor temperature estimation by analyzing the principle of heat generation and heat transferring path inside the motor system during operation based on the conservation of energy for the stator heat consumption and establishing a numerical model of rotor temperature estimation by experiment. Different constant load power is adopted to motor real operation states at different environment temperatures and the numerical model of total cooling power is optimized by comparing rotor temperature errors between real test and model calculation to improve the estimation accuracy of the rotor temperature model. Then, the model estimation accuracy of rotor temperature is validated at different environment temperatures and variational load power, and the test result shows that dynamic estimation accuracy between measurement and estimation is within ±5°C. According to the high accuracy estimation of rotor temperature in this research, duration operation time of motor peak power can be significantly expanded because the protection threshold of rotor temperature is increased to improve the peak performance of motor in electric vehicle.

## Data Availability

All data used to support the findings of this study are available from the corresponding author upon request.

## Conflicts of Interest

The authors declare that they have no conflicts of interest.

## Acknowledgments

## References

[1] I. Boldea, L. N. Tutelea, L. Parsa, and D. Dorrell, "Automotive electric propulsion systems with reduced or no permanent magnets: an overview," *IEEE Transactions on Industrial Electronics*, vol. 61, no. 10, pp. 5696–5711, 2014.

[2] H. Liang, Y. Chen, S. Liang, and C. Wang, "Fault detection of stator inter-turn short-circuit in PMSM on stator current and vibration signal," *Applied Sciences*, vol. 8, no. 9, p. 1677, 2018.

[3] D. Huang, W. Li, Y. Wang, and Z. Cao, "Influence of magnetic slot wedge on rotor losses and temperature field of PMSM," *Electric Machines and Control.Magnetics*, vol. 20, pp. 60–66, 2016.

[4] Y. Chen, S. Liang, W. Li, H. Liang, and C. Wang, "Faults and diagnosis methods of permanent magnet synchronous motors: a review," *Applied Sciences*, vol. 9, no. 10, p. 2116, 2019.

[5] W. Li, Y. Chen, X. Li, and S. Liang, "Matching quality detection system of synchronizer ring and cone," *Applied Sciences*, vol. 9, no. 17, p. 3622, 2019.

[6] J. Dong, Y. Huang, L. Jin et al., "Thermal optimization of high-speed permanent motor," *IEEE Transactions on Magnetics*, vol. 50, Article ID 7018504, 2014.

[7] K.-S. Kim, B.-H. Lee, and H.-J. Kim, "Thermal analysis of outer rotor type IPMSM using thermal equivalent circuit," in *Proceedings of the 15th International Conference on Electrical Machines and Systems*, pp. 1–4, Sapporo, Japan, October 2012.

[8] Y. Liu, J. Li, Z. Chen, D. Qin, and Y. Zhang, "Research on a multi-objective hierarchical prediction energy management strategy for range extended fuel cell vehicles," *Journal of Power Sources*, vol. 429, pp. 55–66, 2019.

[9] N. Rostami, M. R. Feyzi, J. Pyrhonen, A. Parviainen, and M. Niemela, "Lumped-parameter thermal model for axial flux permanent magnet machines," *IEEE Transactions on Magnetics*, vol. 49, no. 3, pp. 1178–1184, 2013.

[10] J. D. McFarl and T. M. Jahns, "Investigation of the rotor demagnetization characteristics of interior PM synchronous machines during fault conditions," *IEEE Transactions on Industry Applications*, vol. 50, pp. 2768–2775, 2013.

[11] T. Reichert, T. Nussbaumer, and J. W. Kolar, "Split ratio optimization for high-torque PM motors considering global and local thermal limitations," *IEEE Transactions on Energy Conversion*, vol. 28, no. 3, pp. 493–501, 2013.

[12] K.-C. Kim and D.-S. Ryu, "Torque characteristic with respect to the load angle of a permanent magnet motor," *IEEE Transactions on Magnetics*, vol. 48, no. 11, pp. 4200–4203, 2012.

[13] X. Jannot, J.-C. Vannier, C. Marchand, M. Gabsi, J. Saint-Michel, and D. Sadarnac, "Multiphysic modeling of a high-speed interior permanent-magnet synchronous machine for a multiobjective optimal design," *IEEE Transactions on Energy Conversion*, vol. 26, no. 2, pp. 457–467, 2011.

[14] L. Guangjin, J. Ojeda, E. Hoang et al., "Thermal-electro-magnetic analysis for driving cycles of embedded flux-switching permanent-magnet motors vehicular technology," *IEEE Transactions on Magnetics*, vol. 61, pp. 140–151, 2012.

[15] D. Joo, J.-H. Cho, K. Woo, B.-T. Kim, and D.-K. Kim, "Electromagnetic field and thermal linked analysis of interior permanent-magnet synchronous motor for agricultural electric vehicle," *IEEE Transactions on Magnetics*, vol. 47, no. 10, pp. 4242–4245, 2011.

[16] D. H. Lim and S. C. Kim, "Thermal performance of oil spray cooling system for in-wheel motor in electric vehicles," *Applied Thermal Engineering*, vol. 63, no. 2, pp. 577–587, 2014.

[17] T. Deng, Z. Su, J. Li et al., "Advanced angle field weakening control strategy of permanent magnet synchronous motor," *System Control Engineering*, vol. 68, pp. 3425–3435, 2019.

[18] Y. Xie, Z. Wang, X. Shan, and Y. Li, "The calculations and analysis of 3D transient magnetic-thermal-solid coupling for squirrel-cage induction motors based on multi fields," *Proceedings of the CSEE.Magnetics*, vol. 36, pp. 3076–3084, 2016.

[19] X. Sun, Y. Shen, S. Wang, G. Lei, Z. Yang, and S. Han, "Core losses analysis of a novel 16/10 segmented rotor switched reluctance BSG motor for HEVs using nonlinear lumped parameter equivalent circuit model," *IEEE/ASME Transactions on Mechatronics*, vol. 23, no. 2, pp. 747–757, 2018.

[20] X. Sun, Z. Shi, G. Lei, Y. Guo, and J. Zhu, "Analysis and design optimization of a permanent magnet synchronous motor for a campus patrol electric vehicle," *IEEE Transactions on Vehicular Technology*, vol. 68, no. 11, pp. 10535–10544, 2019.

[21] N. Yang, M. Zhang, B. Guo, and C. Xiao, "Analysis of temperature field in ironless stator axial field permanent motor," *Computer Simulation Magnetics*, vol. 32, pp. 259–263, 2015.

[22] L. Chen, W. Zhao, and J. Ji, "Thermal analysis and calculation of fault-tolerant permanent magnet machine by using equivalent thermal network method," *Magnetics*, vol. 43, pp. 45–50, 2016.

[23] C. Li, F.-C. Huang, and Y.-Q. Wang, "An applicable real-time thermal model for temperature prediction of permanent magnet synchronous motor," *Proceedings of the Institution of Mechanical Engineers, Part I: Journal of Systems and Control Engineering*, vol. 231, no. 1, pp. 43–51, 2017.

[24] H. Toda, K. Senda, S. Morimoto, and T. Hiratani, "Influence of various non-oriented electrical steels on motor efficiency and iron loss in switched reluctance motor," *IEEE Transactions on Magnetics*, vol. 49, no. 7, pp. 3850–3853, 2013.

[25] A. Boglietti, A. Cavagnino, and M. Lazzari, "Fast method for the iron loss prediction in inverter-fed induction motors," *IEEE Transactions on Industry Applications*, vol. 46, no. 2, pp. 806–811, 2010.

[26] J. Nerg, M. Rilla, and J. Pyrhonen, "Thermal analysis of radial-flux electrical machines with a high power density," *IEEE Transactions on Industrial Electronics*, vol. 55, no. 10, pp. 3543–3554, 2008.

[27] C. Li, *Study on the Cooling System for Mini Vehicle Induction Motor.* Harbin Institute of Technology, Harbin, China, 2013.

[28] L. Liu, *The Study of Thermal Characteristics in Various Conditions Cooling System of Permanent Magnet Synchronous Motor in Pure Electric Vehicle*, Hefei University of Technology, Hefei, China, 2015.

[29] H. Liu, L. Yang, and F. Sun, "Study of numerical method determining inner temperature rise of asynchronous motor based on thermographic measurement," *Magnetics*, vol. 27, pp. 496–500, 2006.

[30] W. Li, S. Li, Y. Xie, and S. Ding, "Stator-rotor coupled thermal field numerical calculation of induction motors and correlated factors sensitivity analysis," *Proceedings of the CSEE. Magnetics*, vol. 24, pp. 85–91, 2007.